Proceedings of the IASS 2024 Symposium
Redefining the Art of Structural Design
August 26-30, 2024, Zurich, Switzerland
Philippe Block, Giulia Boller, Catherine DeWolf,
Jacqueline Pauli, Walter Kaufmann (eds.)

Reconfigurable shellular structures assembled from strip modules

Kanata WARISAYA, Tomohiro TACHI*

* The University of Tokyo
Tokyo, 153-8902 Japan
tachi@idea.c.u-tokyo.ac.jp

Abstract

Shellular structures, i.e., cellular structures composed of a single smooth thin shell, have been gaining attention for their unique property such as high stiffness for low density, and division of space into two subvolumes. Since they have negative Gaussian curvature, they cannot be constructed by simply bending sheet material. This study aims to efficiently construct shellular structures from sheet material by assembling a single type of developable pieces. The existing method allows dividing some of the triply periodic minimal surfaces (P, D, and G surfaces) into a single type of narrow strip by periodic geodesic net connecting monkey saddles on them. We apply this division method to P, D, and G surfaces of constant negative Gaussian curvature, a family of tubular surfaces with different slenderness. Due to the intrinsic isometry of the family, some elements of the family can consist of the congruent strip, enabling reconfiguration between surfaces with different topologies or slenderness. We fabricate physical models by approximating the strip with a developable surface. The straight strip allows for a high efficiency of material and can be cut from a roll of sheet. We believe this reconfigurable modular system can be a new geometric basis for self-build and self-assembly assuming disassembly and reconstruction.

Keywords: shellular structure, tessellation, modular construction, reconfiguration, sheet material.

1. Introduction

Background: shellular structures Cellular structures composed of a shell existing in microstructures of some living organisms [1, 2, 3] have recently been named "shellular structures" and attracting attention for their properties such as high stiffness for low density and partitioning space into two subvolumes. They have been applied for engineering purposes such as infill of 3D printing [4], heat exchanger [5], architectural shell [6]. The surfaces composing shellular structures are often expressed as triply periodic minimal surfaces (TPMSs), the unit of minimal surfaces smoothly connecting through the boundary and forming periodic tessellation. Simple examples of TPMSs with cubic symmetry are Schwarz' primitive (P) surface and diamond (D) surface [7], and Schoen's gyroid (G) surface [8]. In each example, the orientable surface divides space into two congruent subvolumes called *labyrinths* [8], whose *skeletal graph* [8] is the cubic graph, the diamond graph, and the Laves graph [9], respectively.

Shellular structures cannot be constructed simply by bending sheet material, due to the negative Gaussian curvature of the surface. Existing works have solved this problem with origami [10] or division into developable pieces [11, 12]. Most of the previous works aim to construct a single type of surface.

Contribution This paper aims to construct multiple types of shellular structures from a single type of piece. First, in Section 3. we explore unexplored families of surfaces of constant negative Gaussian curvature ($K = -1$ surfaces). In particular, we construct one-parameter families of P, D, and G surfaces with varying slenderness that are intrinsically isometric to each other. The slender variations have different volume ratios of two subvolumes and different dimensions of the unit cube, extending the potential

application. For example, in architectural use, the slender variations behave like a lightweight frame. To divide the surfaces, we apply the method proposed by past work in crystallography [13] (reviewed in Section 2.). We extend their method to the families of $K = -1$ surfaces in Section 4.. The method can divide the surfaces into a single type of hyperbolic strips. In Section 5. we indicate the reconfigurable variants, which can be assembled from the same pieces. This is an advantage in fabrication in that we only need to produce one type of strip to construct multiple types of surfaces. Moreover, if the joint system allows for disassembly, the strips can be reused to construct the other surface. Section 6. proposes a flattening method of $K = -1$ strip for fabrication from sheet material. The narrow strip shape can be flattened with a smaller approximation error. Moreover, the strip has a straight center line, allowing for high material efficiency when cutting from a sheet.

2. Review: periodic net on Poincaré disk model and P, D, G surfaces

This section provides the basic mathematical concepts that we use in our construction, namely the method for mapping a grid in hyperbolic plane $\mathbb{H}^2$ to P, D, and G surfaces proposed by Ramsden et al. [14] and drawing periodic geodesic net on them based on the grid as proposed by Evans et al. [13].

2.1. Poincaré disk model

The Poincaré disk model is used to represent $\mathbb{H}^2$ in $\mathbb{E}^2$ in this paper. The model conformally maps $\mathbb{H}^2$ having $K = -1$ in the region of unit circle C, the circle at infinity. In this model, a line (geodesic) is expressed as a circle intersecting orthogonally to C, including the diameters of C.

2.2. Grid of monkey saddles

Ramsden et al. [14] proposed a covering map from $\mathbb{H}^2$ to TPMSs. A regular quadrilateral degree-6 tiling on $\mathbb{H}^2$ (all the internal angles are $\frac{\pi}{3}$) can be mapped to P, D, and G surfaces so that the corners of the quadrilateral are on the monkey saddles of them (Figure 1 Top).

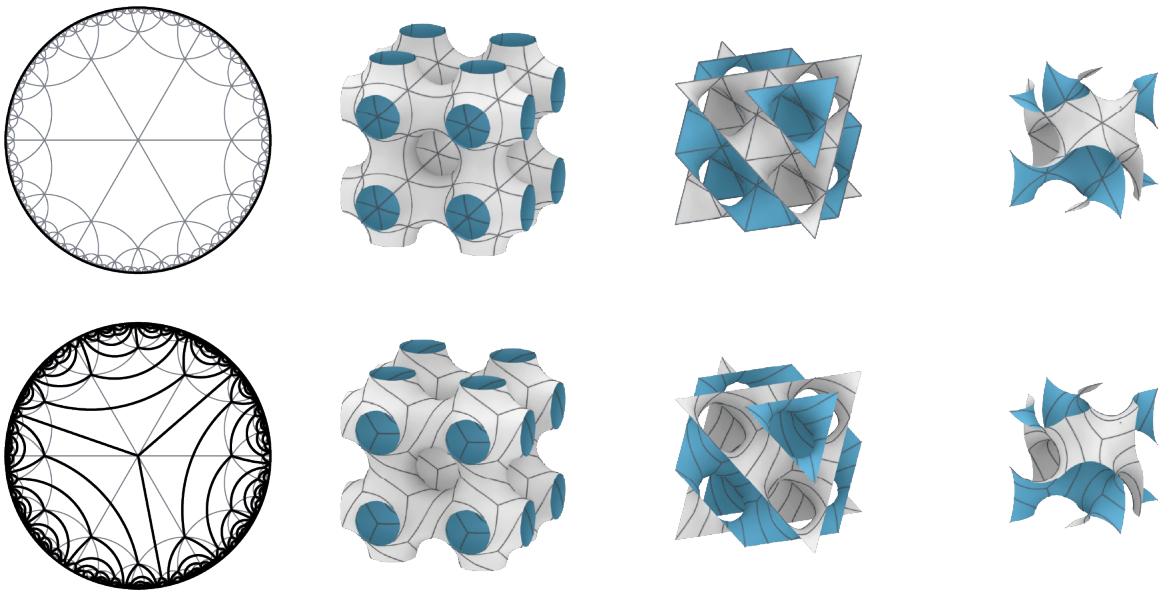

Figure 1: Top: regular quadrilateral tiling of degree-6 on $\mathbb{H}^2$, P, D, and G surfaces (from left to right). Bottom: division $\boldsymbol{d} = \{1, 2\}$ applied to each surface.

2.3. Periodic geodesic net

Evans et al. [13] proposed a division method of P, D, and G surfaces into a single type of strip by connecting pairs of monkey saddles by geodesics. First, the grid points in $\mathbb{H}^2$ contained in $\mathbb{E}^2$ domain are denoted by a pair of integers $\{\mathbb{Z}, \mathbb{Z}\}$ (Figure 2 (a)). Then, a vector connecting two grid points is specified. We call this as *division* $\boldsymbol{d} = \{p, q\}$. $\boldsymbol{d}$ must be chosen so that p and q are a coprime pair. In Figure 2 (b), $\boldsymbol{d} = \{1, 2\}$ is applied, and the geodesic net is colored light blue. In the domain out of $\mathbb{E}^2$ colored gray, geodesics are drawn so that they have 3-fold symmetry at grid points and 2-fold symmetry at the midpoint of them.

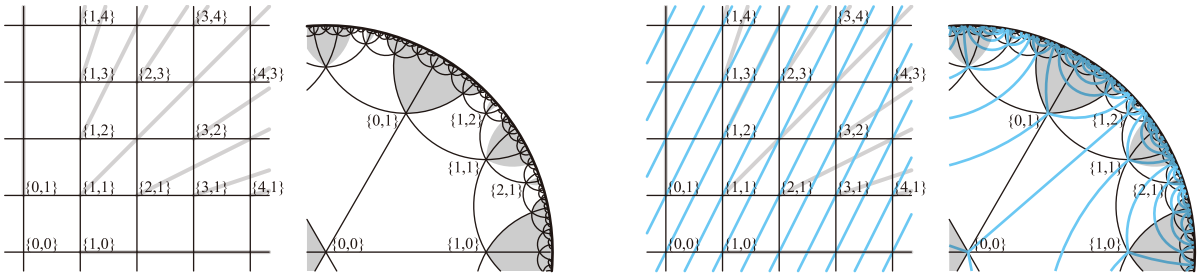

(a) (b)

Figure 2: (a) Notation of grid points in $\mathbb{E}^2$ domain. (b) Geodesic net with $\boldsymbol{d} = \{1, 2\}$ colored light blue.

The strip is composed of unit triangles infinitely tiled by 2-fold symmetry at the midpoints of two edges included in the strip. Moreover, we can take any triangle $\{0, 0\}, \boldsymbol{P} + k\boldsymbol{d}, \boldsymbol{P} + (k + 1)\boldsymbol{d}$ as unit, where $\boldsymbol{P}$ is a corner of the strip on the opposite side of $\{0, 0\}$, and $k \in \mathbb{Z}$, as shown in Figure 3 (a) and (b). Because every corner of the strip has an angle of $\frac{\pi}{3}$ due to the 3-fold symmetry, the sum of internal angles of the unit triangle is constant, $\frac{2}{3}\pi$. In a unit triangle $\{0, 0\}, \boldsymbol{P} + k\boldsymbol{d}, \boldsymbol{P} + (k + 1)\boldsymbol{d}$, the geodesic segment between $\boldsymbol{P} + k\boldsymbol{d}$ and $\boldsymbol{P} + (k + 1)\boldsymbol{d}$ intersects with the Euclid line between them in angle of

$$\frac{\pi - \frac{2}{3}\pi}{2} = \frac{\pi}{6} \tag{1}$$

because the geodesic is represented by circular arc (Figure 3 (c)). As a result, the grid points $\boldsymbol{P} + k\boldsymbol{d}$ at the corners of a strip on the opposite side of $\{0, 0\}$ are colinear. This line also contains inversions of $\boldsymbol{d}$ and $-\boldsymbol{d}$ about C. This colinearity is used to find grids for surfaces varying slenderness in Section 3.1.. The area of the unit triangle is constant $\frac{\pi}{3}$, subtraction of the sum of the internal angles from π, using the fact from hyperbolic geometry. Therefore, a strip with a longer edge has a narrower width.

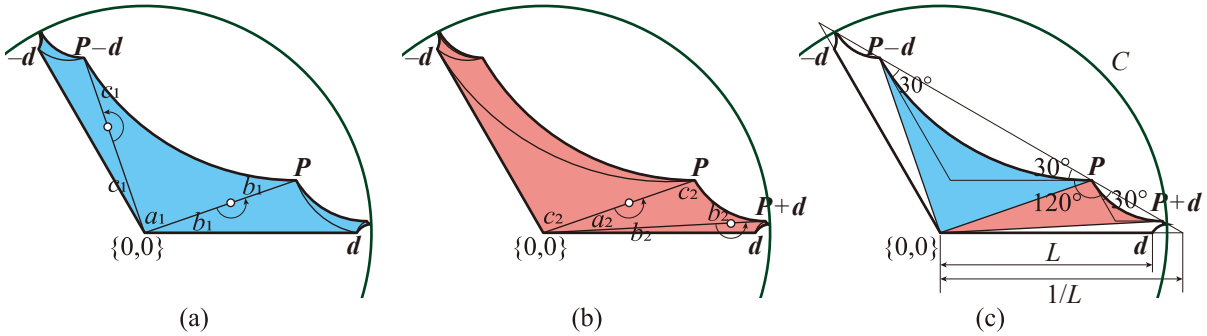

(a) (b) (c)

Figure 3: (a)(b) Strip tiled by unit triangle in two ways. (c) Colinearity of grid points on corner of strip.

3. Isometric family of TPKSs with varying slenderness

To achieve a reconfigurable module, one surface needs to be intrinsically isometric to the other surface. We suppose triply periodic $K = -1$ surfaces (TPKSs), whose isometry is guaranteed by Minding's theorem [15]. In fact, the original minimal P, D, and G surfaces are isometric, allowing for transformation into each other through Bonnet transformation [16], but variations of isometric surfaces are limited. In contrast, TPKSs can vary their slenderness while preserving intrinsic isometry.

3.1. Transforming grids of TPKSs in $\mathbb{H}^2$

We construct P, D, and G surfaces of $K = -1$ by considering an isometric covering map from $\mathbb{H}^2$. To make slender variations, we first reconstruct grids for each surface 'canonically', whose direction coincides with the direction of varying slenderness by a pair of $\boldsymbol{d}$ making the angle of $\frac{\pi}{3}$ shown in Figure 4 top: $\{1,0\},\{0,1\}$ for P surface, $\{1,1\},\{-1,1\}$ for D surface, and $\{1,2\}$ and $\{-2,1\}$ for G surface ($\{2,1\}$ and $\{-1,2\}$ for G surface with the other chirality). The strips make closed rings in each $\boldsymbol{d}$. Let the Euclid distances from $\{0,0\}$ to the pair of $\boldsymbol{d}$ be L and l. L and l are equal in the original grids. Here we transform the grids while varying a ratio of L and l. For the slender surfaces to allow for drawing periodic nets with any $\boldsymbol{d}$ as the original surfaces, the colinearity of the grid points we saw in Section 2.3. must be preserved. We find the following implicit functions of L and l satisfying this nature for P, D, and G surfaces:

$$2Ll - 1 = 0, \tag{2}$$

$$3L^2l^2 + L^2 + l^2 - 4Ll = 0, \tag{3}$$

$$27L^5l^3-54L^4l^4+27L^3l^5+5L^5l-25L^4l^2+48L^3l^3-25L^2l^4+5Ll^5-L^4+5L^3l-15L^2l^2+5Ll^3-l^4 = 0, \tag{4}$$

respectively. Figure 4 bottom shows the transformed grids.

These functions are plotted in Figure 5 left. Now let the length of these geodesics be L_H and l_H. Using the formula for hyperbolic distance from the center of C,

$$L_H = 2\tanh^{-1}(L). \tag{5}$$

We plotted functions of L_H and l_H obtained by replacing L and l in Equation 2, 3, and 4 by L_H and l_H (Figure 5 right). We regard the ratio $\frac{L_H}{l_H}$ as the *slenderness* of the surface and denote it by s:

$$s = \frac{L_H}{l_H} = \frac{\tanh^{-1}(L)}{\tanh^{-1}(l)}. \tag{6}$$

A pair of surfaces with inverse slenderness $s, \frac{1}{s}$ are congruent with opposite normal directions.

3.2. Immersion of TPKSs in $\mathbb{E}^3$

We immerse the surfaces in $\mathbb{E}^3$ through numerical simulation. First, as the initial configurations, we provide polyhedra homeomorphic to P, D, and G surfaces whose faces compose a grid covered from the canonical grid constructed in Section 3.1.. The polyhedra for P and D surfaces can be provided by removing specific faces from the tessellation of cubes (known as the regular skew polyhedron $\{4,6|4\}$) and rhombic dodecahedra, respectively. For G surfaces we use the polyhedron discovered by Norman Johnson [17]. These polyhedra allow for varying s as the smooth surfaces; using polyhedra of the target s can stabilize the simulation. Then, we subdivide the minimum unit of both the grid on $\mathbb{H}^2$ and the corresponding faces of the polyhedra into triangulated meshes, M_H in $\mathbb{H}^2$ and M_0 in $\mathbb{E}^3$ (Figure 6 (a),

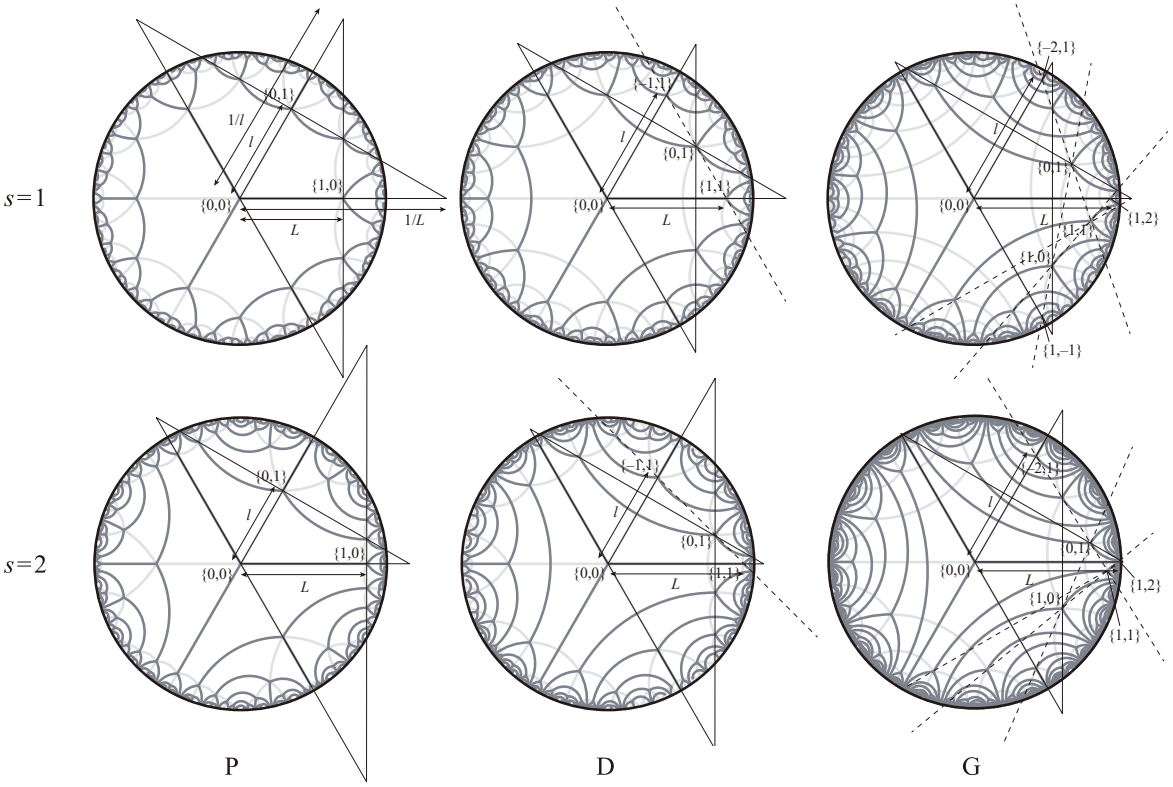

Figure 4: Canonical grids of P, D, and G surfaces of $s = 1$ (top) and $s = 2$ (bottom). Grids are composed of a pair of geodesic nets colored dark gray and light gray.

(b)). Finally, we impose the following constraints on the unit face M_0, the adjacent quads $M_i = T_i(M_0)$ transformed using the global symmetry, and a mesh M_{all} combining M_0 and all the M_i.

C1 $V_i = T_i(V_0)$;

C2 $E_0 = kE_H$ with some constant k;

C3 The angles between adjacent faces of M_{all} are 0,

where V_* is the set of vertices of M_*, and E_* is the set of edges of M_*. C1 is for the global symmetry of the surface. C2 is for similarity between M_H and M_0. C3 is for the smoothness of the surface. Among these, C1 must be strictly satisfied, but C3 must not be strictly satisfied. We obtained a configuration satisfying these constraints by minimizing the sum of their potential energy U:

$$U := w_{C1} * U_{C1} + w_{C2} * U_{C2} + w_{C3} * U_{C3} \tag{7}$$

where U_* is the potential energy of constraint $*$, and w_* is the weight of U_*. w_* are set so that $w_{C1} > w_{C2} >> w_{C3}$. We solved this problem as dynamic relaxation of a mass-spring system using Kangaroo 2 [18] on Grasshopper. C1, C2, C3 are implemented using *Transform Goal*, *LengthRatio Goal*, *Hinge Goal*, respectively. The resulting surface is a scaled surface with the factor of k, so we finally scale the surface by $\frac{1}{k}$. While varying s, the dimension of the unit cube and volume ratio of the two subvolumes also vary. We only confirmed the existence of TPKSs by numerical simulation. Note that Hilbert's theorem [19] states that there is no complete $K = -1$ surface with C^2 continuity immersed in $\mathbb{E}^3$. We allow for the periodic monkey saddles where the surface has C^1 continuity. Whether or not there are no other points with C^1 continuity is not yet revealed.

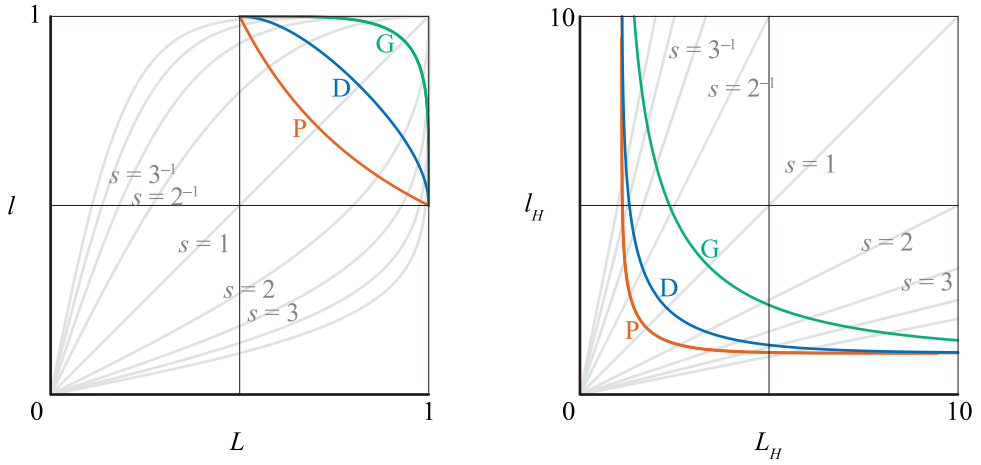

Figure 5: Functions of L and l (left) and L_H and l_H (right) for each surface. The intersections with gray curves are the states with specific s.

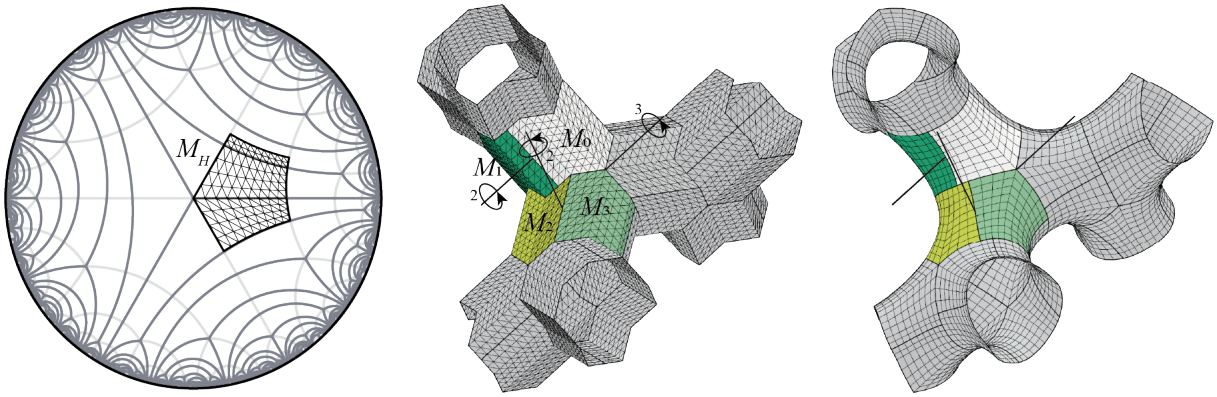

(a) (b) (c)

Figure 6: Constructing G surface of $s = 2$ in $\mathbb{E}^3$ thorough simulation. (a) Unit faces in $\mathbb{H}^2$. (b) Initial configuration. (c) Final configuration.

4. Division

While varying the parameter s of TPKSs, the grid points of monkey saddles transform as shown in Figure 4. We apply the method [13] reviewed in Section 2. to the transformed grid to divide the surfaces into a single type of strip. Figure 7 shows the surfaces of $s = 2$ divided in $\boldsymbol{d} = \{1, 2\}$.

5. Reconfigurability

This section finds reconfigurable surfaces from the surfaces divided in Section 4. by evaluating the congruence of the strip. Due to the intrinsic isometry among $K = -1$ surfaces, strips are congruent if their boundary curves drawn on the disk coincide. Figure 8 (a) shows the parameters of strip configuration. Let the center of C be O, and the corners of the strip on the opposite side of O be $P_k (k \in \mathbb{Z})$, and the hyperbolic midpoint of OP_k be M_k. Then, the hyperbolic distance x_H between M_k and M_{k+1} is constant for any choice of k, due to the periodicity of the strip. By connecting M_k and M_{k+1} by a geodesic, the *center line* m of the strip can be drawn.

Let the angle bisector of two edges of the strip starting from O be n, and the intersection of m and n be N. Then, let the signed hyperbolic distance between M_k and N be $y_{H,k}$ (positive if z component of

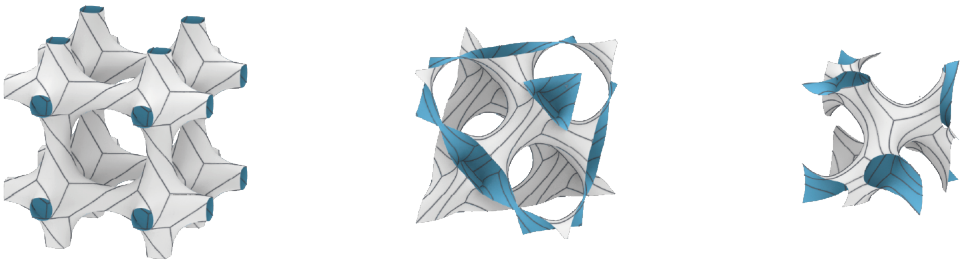

Figure 7: P, D, G surfaces of $s = 2$ divided in $\{1, 2\}$ (from left to right).

$\overrightarrow{OM_k} \times \overrightarrow{ON}$ is positive). Here, we take

$$y_H = y_{H,k} \bmod x_H. \tag{8}$$

The strip configuration can be determined by the two parameters x_H and y_H. x_H represents the length of the unit of the strip. The width of the strip is also determined by x_H due to the area-preserving property shown in Section 2.3.. y_H represents the difference in 'phase' of the two opposite sides of the strip. We plot the strip configuration with the horizontal axis x_H and the vertical axis $\frac{y_H}{x_H} \in [0, 1]$ (Figure 9). The surfaces are reconfigurable at the intersections of the curves, where the strip configurations are congruent. We find the plots have periodicity; intersections representing the same pair of surfaces repeatedly appear. It revealed that the reconfigurable sets of surfaces share all the grid points on $\mathbb{H}^2$ (Figure 10). Thus they allow for choices of $\boldsymbol{d}$. Choosing $\boldsymbol{d}$ closer to $\{0, 0\}$ makes a wider strip, and choosing $\boldsymbol{d}$ farther from $\{0, 0\}$ makes a narrower strip. The narrower the strip, the longer the edges to be connected (and the assembly time). On the other hand, when approximating the strip by a flat surface, a narrower strip has less approximation error, discussed in Section 6.3..

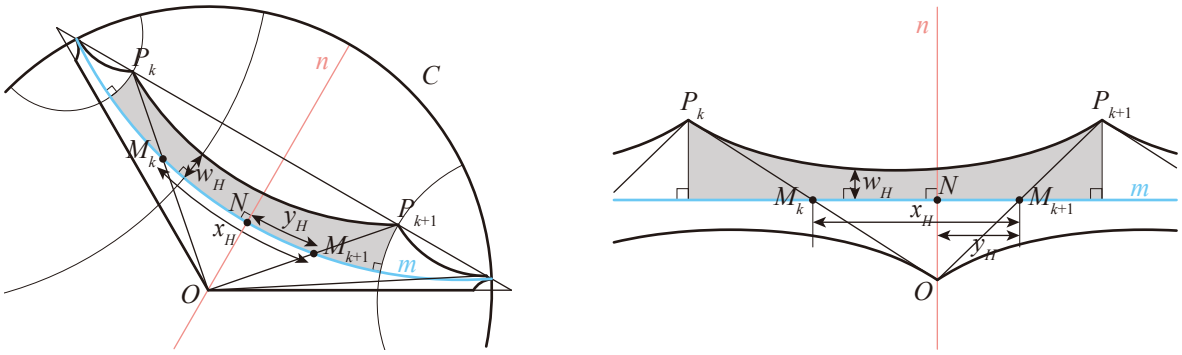

(a) (b)

Figure 8: (a) Parameters x_H and y_H representing the strip configuration. (b) Flattened strip.

6. Fabrication from sheet material

6.1. Flattening $K = -1$ strip

We consider the approximation of the $K = -1$ strip obtained in Section 4. by a developable $K = 0$ strip. If the target surface is just one, the strip can be developablized with a better approximation by constructing rulings in the conjugate direction of the geodesic divisor. However, if there are multiple target surfaces, their conjugate direction is generically different. Therefore, we propose flattening method neutrally works for every $\boldsymbol{d}$. See Figure 8. First, in $\mathbb{E}^2$, we straighten m isometrically. The center of

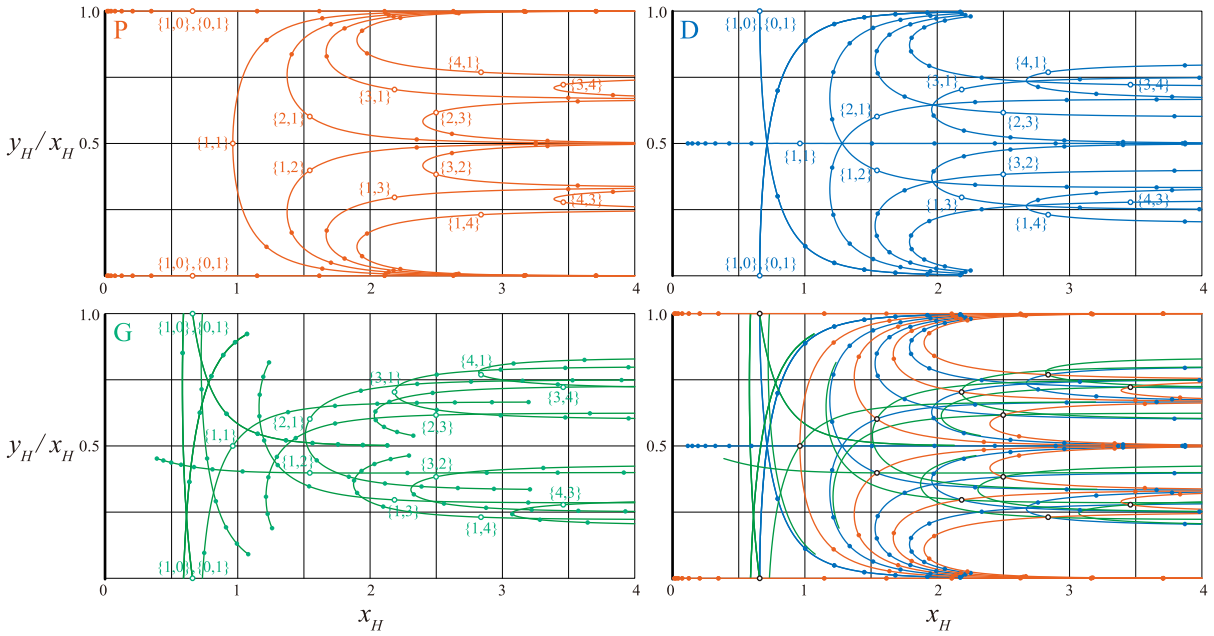

Figure 9: Plots of strip configuration. Surfaces are reconfigurable at intersections.

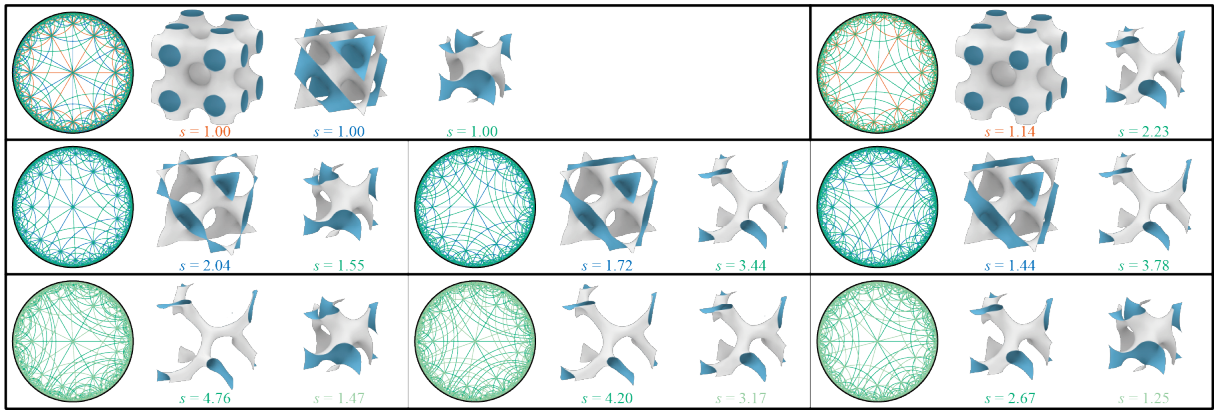

Figure 10: Reconfigurable sets of surfaces. Each set shares grid points in $\mathbb{H}^2$.

rotational symmetry M_k can be mapped together. Then, in $\mathbb{H}^2$, we measure the width of the strip w_H between m and the boundary in the direction orthogonal to m, in the range of a unit of the symmetry (colored gray). Finally, in $\mathbb{E}^2$, the boundary curve of the unit can be constructed by taking points distant from m by w_H. All the boundary curves can be drawn with the rotation about M_k. A flat strip with the straight center line can be cut from a sheet with high material efficiency. A roll sheet can also be used.

6.2. Assembly

Edge-edge connection We made physical models by connecting strips at the edges (Figure 11). We equally divided the boundary by an even number and added joinery (a). The strips are laser-cut from ALPHAYUPO [20] with $t = 0.5\,\mathrm{mm}$ and assembled into D and G surfaces with $s = 1, \boldsymbol{d} = \{3, 2\}$ (b).

Face-face connection We can divide a surface in two different $\boldsymbol{d}$ and use them as two layers. In this case, the strips can be joined at their faces. Strips can also be woven if the sheet is sufficiently thin because the grid becomes two-colorable with all the vertices having degrees of even numbers: degree-4 vertices at the intersection of two geodesics and degree-6 vertices at the monkey saddles.

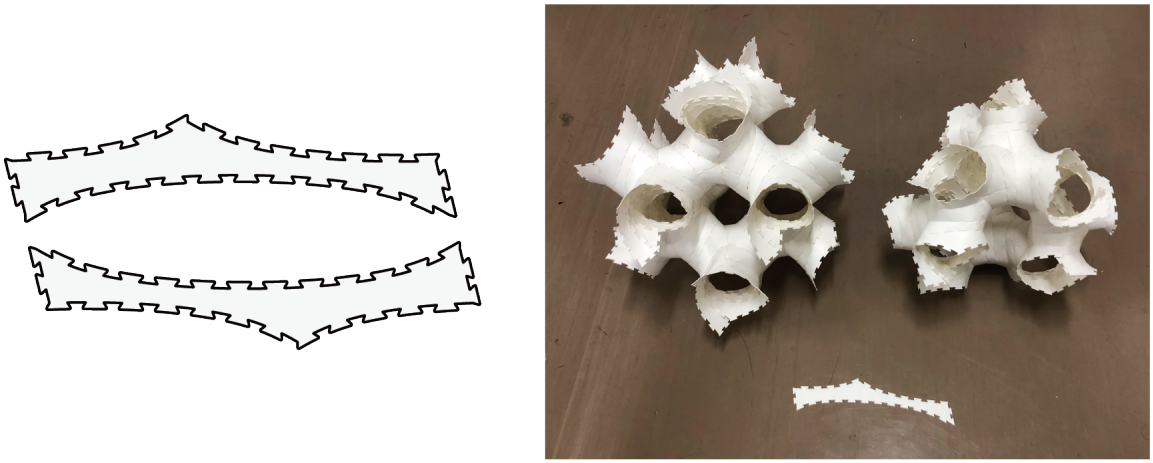

(a) (b)

Figure 11: (a) Strip with joinery. (b) Physical models of D and G surfaces from single type of strip.

6.3. Discussion: accuracy of approximation

Our flattening of the strip maintains the length in the width direction but ignores the stretch in the length direction that occurs as distant from m (Figure 8). The stretching factor $r(w_H)$ can be expressed as

$$r(w_H) = \cosh(w_H), \tag{9}$$

referring to the parameterization of a $K = -1$ surface of hyperboloid type [21]. Therefore, the strain ϵ in the length direction increases exponentially as w_H increases:

$$\epsilon = \frac{r(w_H) - r(0)}{r(0)} = \cosh(w_H) - 1. \tag{10}$$

As the strip gets longer, the maximum Euclid width ON in Figure 8 (a) converges to $2 - \sqrt{3}$, and ϵ converges to $\frac{2}{\sqrt{3}} - 1 \sim 0.1547$. In actual construction, the resulting surface is not a $K = -1$ surface but a surface determined by the balance between bending and in-plane deformations.

7. Conclusion

We proposed a method for constructing the family of P, D, and G surfaces of $K = -1$ with varying slenderness and divided them into a single type of strip. By utilizing the intrinsic isometry of the family, we revealed the reconfigurable sets of surfaces that can be assembled from congruent strips. We approximated the strip by developable surfaces to fabricate from sheet material. We believe this reconfigurable modular system can be a new geometric basis for self-build or self-assembly. For example, it can be applied to temporary frame or shell structures assuming disassembly and reconstruction, or concrete formwork for more permanent structures. The local connection of strips does not determine the global shape of the surface; for easier assembly, we need to establish a notation method that contains information on a global connection. Also, this paper only shows smooth surfaces to be divided and does not investigate the behavior of the piecewise-developable model. This remains the future work of our study.

Acknowledgments

This work is supported by JST AdCORP "Realization of people- and environment-friendly artifacts by leveraging computational design and fabrication".

References

[1] G. Donnay and D. L. Pawson, "X-ray diffraction studies of echinoderm plates," *Science*, vol. 166, no. 3909, pp. 1147–1150, 1969.

[2] K. Michielsen and D. G. Stavenga, "Gyroid cuticular structures in butterfly wing scales: Biological photonic crystals," *Journal of The Royal Society Interface*, vol. 5, no. 18, pp. 85–94, 2008.

[3] T. Yang *et al.*, "A damage-tolerant, dual-scale, single-crystalline microlattice in the knobby starfish, protoreaster nodosus," *Science*, vol. 375, no. 6581, pp. 647–652, 2022.

[4] J. Podroužek, M. Marcon, K. Ninčević, and R. Wan-Wendner, "Bio-inspired 3d infill patterns for additive manufacturing and structural applications," *Materials*, vol. 12, no. 3, p. 499, 2019.

[5] Nature Architects Inc, *Structure*, JP2022151825A, Oct. 2022.

[6] Toyo Ito & Associates, Architects, *National taichung theater*, http://www.toyo-ito.co.jp/WWW/Project_Descript/2015-/2015-p_04/2015-p_04_en.html.

[7] H. A. Schwarz, "Gesammelte mathematische abhandlungen," *Berlin J. Springer*, vol. 1, 1890.

[8] A. H. Schoen, "Infinite periodic minimal surfaces without self-intersections," Tech. Rep., 1970.

[9] F. Laves, "Zur klassifikation der silikate. geometrische untersuchungen möglicher silicium-sauerstoff-verbände als verknüpfungsmöglichkeiten regulärer tetraeder," *Zeitschrift für Kristallographie - Crystalline Materials*, vol. 82, pp. 1–14, 1932.

[10] M. Akbari, Y. Lu, and M. Akbarzadeh, "From design to the fabrication of shellular funicular structures," *Proceedings of the Association for Computer-Aided Design in Architecture (ACADIA)*, 2021.

[11] NERVOUS SYSTEM, *Yellow moon gyroid*, https://n-e-r-v-o-u-s.com/blog/?p=9176, 2022.

[12] M. Fornes, *Marc fornes / theverymany*, https://theverymany.com/project-gallery.

[13] M. E. Evans, V. Robins, and S. T. Hyde, "Periodic entanglement i: Networks from hyperbolic reticulations," *Acta Crystallographica Section A*, vol. 69, pp. 241–261, 2013.

[14] S. Ramsden, V. Robins, and S. Hyde, "Three-dimensional euclidean nets from two-dimensional hyperbolic tilings: Kaleidoscopic examples," *Acta crystallographica. Section A, Foundations of crystallography*, vol. 65, pp. 81–108, Mar. 2009. DOI: 10.1107/S0108767308040592.

[15] F. Minding, "Wie sich entscheiden lässt, ob zwei gegebene krumme flächen auf einander abwickelbar sind oder nicht; nebst bemerkungen über die flächen von unveränderlichem krümmungsmaaße.," ger, *Journal für die reine und angewandte Mathematik*, vol. 19, pp. 370–387, 1839.

[16] O. Bonnet, "Note sur la theorie generale des surfaces," *C R Acad Sci Paris*, vol. 37, pp. 529–532, 1853.

[17] A. H. Schoen, *Triply-periodic minimal surfaces (tpms)*, https://schoengeometry.com/e-tpms.html.

[18] D. Piker, *Kangaroo 2*, https://github.com/Dan-Piker/K2Goals, 2015.

[19] D. Hilbert, "Ueber flächen von constanter gaussscher krümmung," *Transactions of the American mathematical Society*, vol. 2, no. 1, pp. 87–99, 1901.

[20] YUPO CORPORATION, *Alphayupo*, https://japan.yupo.com/english/product/category/thick/.

[21] D. J. Struik, *Lectures on classical differential geometry*. Courier Corporation, 1961.